

NaviSTAR: Socially Aware Robot Navigation with Hybrid Spatio-Temporal Graph Transformer and Preference Learning

Weizheng Wang¹, Ruiqi Wang¹, Le Mao², and Byung-Cheol Min¹

Abstract—Developing robotic technologies for use in human society requires ensuring the safety of robots’ navigation behaviors while adhering to pedestrians’ expectations and social norms. However, maintaining real-time communication between robots and pedestrians to avoid collisions can be challenging. To address these challenges, we propose a novel socially-aware navigation benchmark called NaviSTAR, which utilizes a hybrid Spatio-Temporal grAph tRansformer (STAR) to understand interactions in human-rich environments fusing potential crowd multi-modal information. We leverage off-policy reinforcement learning algorithm with preference learning to train a policy and a reward function network with supervisor guidance. Additionally, we design a social score function to evaluate the overall performance of social navigation. To compare, we train and test our algorithm and other state-of-the-art methods in both simulator and real-world scenarios independently. Our results show that NaviSTAR outperforms previous methods with outstanding performance¹.

I. INTRODUCTION

Recent advances in machine intelligence have led to the integration of robots into human daily life. Service robots are being used in homes, and delivery robots are being deployed in towns, among other applications. This integration requires robots to perform socially aware navigation in spaces shared with humans. Specifically, when navigating in a human-filled environment, robots must not only avoid collisions but also behave in a socially compliant manner, regulating their movements to create and maintain a pleasant spatial interaction experience for human pedestrians [1].

Existing works for socially aware robot navigation can generally be divided into two mainstreams: *decoupled* and *coupled*. Decoupled approaches involve building a model that encodes and predicts crowd dynamics to provide spatial information, such as intentional paths of humans, which then serve as extra parameters of traditional collision-free path planners to generate optimal trajectories [2], [3]. However, such methods ignore latent human-robot interactions, leading to an uncertainty explosion, especially in highly complex environments. Additionally, the freezing robot and reciprocal dance problems can arise [4].

As alternatives, coupled approaches have achieved better performance by approaching the socially aware navigation problem as a Markov Decision Process (MDP) and utilizing

¹SMART Laboratory, Department of Computer and Information Technology, Purdue University, West Lafayette, IN, USA. [wang5716, wang5357, minb]@purdue.edu.

²College of Mechanical and Electrical Engineering, Beijing University of Chemical Technology, Beijing, China. 2020030286@buct.edu.cn.

¹The source code and experiment videos of this work are available at: <https://sites.google.com/view/san-navistar>.

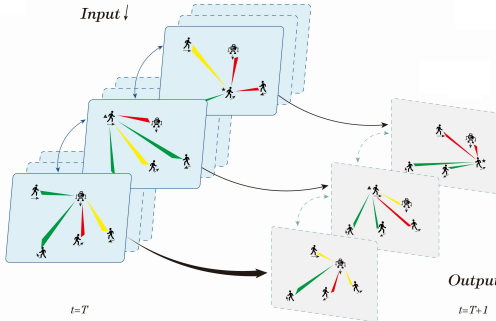


Fig. 1: NaviSTAR uses a hybrid spatio-temporal graph transformer to capture complex environmental dynamics, which aggregates all the spatial and temporal attention maps from each agent.

Reinforcement Learning (RL) to find the optimal robot policy in an end-to-end manner [5]–[11]. Specifically, in the RL framework, a state network is built to learn a state representation that implicitly considers the interactions among agents, including humans and the robot. This representation is then passed through a policy network to learn socially acceptable navigation actions.

Despite the promising results of these approaches, there are still several limitations that need to be addressed. For instance, interaction state representation learning involves highly complex interactions between crowds and robots, including human-human interactions (HHI) and human-robot interactions (HRI), each of which has both spatial and temporal features. Moreover, decision-making is not only driven by these interactions, but also by the latent dependencies across them. However, previous studies have either failed to fully consider the aforementioned interactions in both spatial and temporal dimensions [6]–[9], or failed to efficiently capture the hidden dependencies across multi-modal interactions [12]. On the other hand, for policy learning, most studies tend to rely on a handcrafted reward function, which is difficult to quantify broad social compliance and can lead to the reward exploitation problem when optimizing the robot policy. While the most recent study [11] has shown that active preference learning, which distills the reward model from human feedback, can lead to more preferred and natural robot actions, it still requires a high volume of human efforts to be reasonable.

To address the aforementioned gaps, we propose NaviSTAR, a Spatio-Temporal grAph tRansformer-based model with preference learning. Specifically, we introduce a hybrid spatio-temporal graph transformer structure to encode the latent dependencies across HHI and HRI in both spatial and temporal dimensions into the interaction state representation

(Fig. 1). Then we combine off-policy RL with preference learning to introduce human intelligence and expectations into the reward model with fewer human efforts required.

The main contributions of this paper can be summarized as: 1) We introduce a fully connected spatio-temporal graph to model human-human and human-robot interactions in both spatial and temporal dimensions, and then a hybrid spatio-temporal graph transformer to parallelly capture and encode latent dependencies across into the state representation; 2) We combine off-policy learning and preference learning to train a robot policy with norms and human expectations incorporated; and 3) We conducted extensive simulation experiments and a real-world user study to demonstrate the benefits of our model and each module inside.

II. BACKGROUND

A. Related Works

Deep reinforcement learning (RL) based approaches that treat pedestrians as agents with individual policies to unfold a non-communication multi-agent system have been shown to achieve better performance in socially aware robot navigation. In optimizing robot trajectories for social compliance, a RL framework consists of two parts: 1) a state representation learning network and 2) a policy learning network. The first part implicitly learns the interactions and cooperation among agents and the following part optimizes a robot navigation policy based on the learned state representation. To encode agent interactions, many research efforts have been conducted. For example, [6] introduced a pair-wise navigation algorithm to present the interaction between a pair-wise human and robot, then [7] developed an attention mechanism to cover crowd interactions inside. Furthermore, [8] used a graph convolution network to improve the presentation of HRI as a spatial graph and predict navigation strategies by model-based RL. However, such three studies overlook the temporal features of HHI and HRI. More recently, [9], [12] created a graph of social environments by borrowing temporal edges to comprehensively describe the potential correlation of a multi-agent system. While this method integrates both spatial and temporal features of HHI and HRI, it fails to sufficiently model latent spatio-temporal dependencies.

On the other hand, fewer studies have been conducted to improve the model from the policy learning perspective. Most of them either rely on handcrafted reward function or inverse RL for policy learning. However, the handcrafted reward functions are hard to quantify complex and broad social norms and can result in the reward exploitation problem that leads to unnatural robot behaviors [11]. Moreover, while inverse RL can introduce human expectations to robot policy through demonstrations, it suffers from expensive and inaccurate demonstrations as well as extensive feature engineering. To address these limitations, [11] proposed an active preference learning to tailor a reward model by human feedback, leading to more preferred and natural robot actions. However, it still requires a high volume of human efforts to be reasonable.

B. Spatio-Temporal Graph and Multi Modal Transformer

The spatio-temporal graph (ST-graph) is a conditional random field that captures high-level semantic dependence among objects. ST-graphs present spatial-temporal interactions through edges between nodes, with nodes representing the objects. For example, [13] predicted pedestrian trajectories with an ST-graph, [14] used an ST-graph for Bird's-Eye-View maps, and [15] utilized an ST-graph for traffic flow forecasting. These works demonstrate the powerful feature representation of ST-graphs and the success of transformer-based sequence learning in time series forecasting. And the model of pedestrians' movements is highly spatial-temporal feature-dependent, which is not only rely on surrounding obstacles distribution or spatial interaction, but also can be predicted from trajectory temporal dependencies.

To fuse cross-modal features, a multi-modal transformer was introduced to bridge the gap between heterogeneous modalities. For example, [16] designed a multi-modal transformer to align human speech from vision, language, and audio modalities, while [17] formulated a multi-modal transformer in computational pathology to learn the mapping between medical images and genomic features. Recently, [18] proposed a human state prediction approach using a multi-modal transformer with multi-sensor data.

Inspired by these works, we adapt a spatio-temporal graph transformer to capture long-term dependencies in socially aware navigation tasks that describe the spatial-temporal human-robot interaction. And then aggregate the spatial-temporal dependencies into a multi-modal transformer network to estimate potential cooperation and collision avoidance considering the multimodality and uncertainty of pedestrian movements.

III. METHODOLOGY

A. Preliminaries

Following previous works [6], [7], [9], we define the socially aware navigation task as a partially observable Markov decision process (POMDP) represented by a tuple $\langle \mathcal{S}, \mathcal{A}, \mathcal{O}, \hat{\mathcal{P}}, \mathcal{R}, \gamma, n, \mathcal{S}_0 \rangle$, where n is the number of agents. $\mathbf{s}_t^{jn} \in \mathcal{S}$ represents the joint state of MDP at timestep t , with $\mathbf{s}_t^{jn} = [\mathbf{s}_t^{\text{robot}}, \mathbf{s}_t^{\text{ho}}]$. For each agent, the state is $\mathbf{s}_t = [\mathbf{s}^o, \mathbf{s}^{uo}]$, where $\mathbf{s}^o = [p_x, p_y, v_x, v_y, \text{radius}] \in \mathcal{O}$, represents the observable state, which includes position, velocity, and radius. The hidden state $\mathbf{s}^{uo} = [p_x, p_y, v_{\text{pref}}, \theta]$ contains the agent's self-goal, preferred speed, heading angle. The v_{pref} is used as a normalization term in the discount factor for numerical reasons [6]. The robot action $\mathbf{a}_t \in \mathcal{A}$, and $\hat{\mathcal{P}}$ represents the state transition of the environment. The discount factor γ is in the range [0,1]. \mathcal{R} is the reward function, which, in our algorithm, is represented by a network with parameter α . The initial state distribution is \mathcal{S}_0 . Finally, the objective \mathcal{J} is defined as follows:

$$\mathcal{J}(\pi) = \mathbb{E}(a, s) \left[\sum_t \gamma^{t \cdot v_{\text{pref}}} \cdot \tilde{r}_\alpha(\mathbf{s}_t, \mathbf{a}_t) \right]. \quad (1)$$

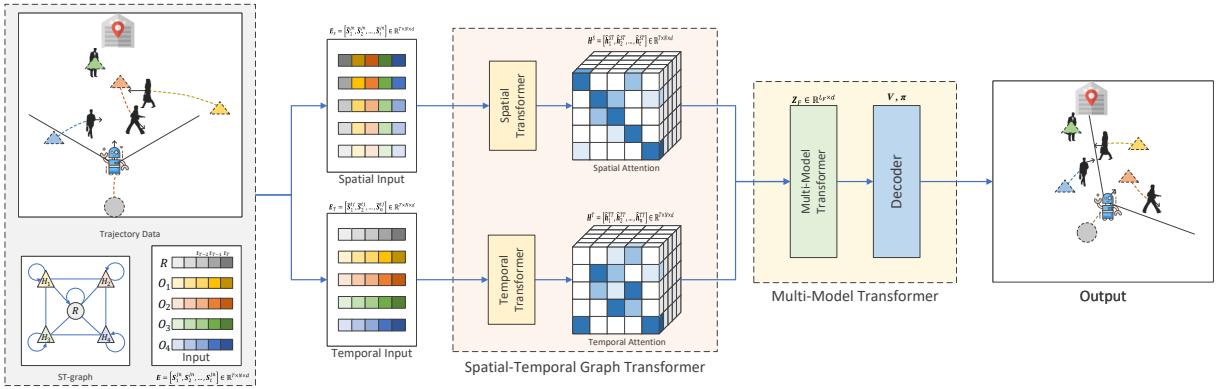


Fig. 2: NaviSTAR architecture: The social navigation planner utilizes a spatial-temporal graph transformer block and a multi-modal transformer block to abstract environmental dynamics and human-robot interactions into an ST-graph for safe path planning in crowd-filled environments. The spatial transformer is designed to capture hybrid spatial interactions and generate spatial attention maps, while the temporal transformer presents long-term temporal dependencies and creates temporal attention maps. The multi-modal transformer is deployed to adapt to the uncertainty of multi-modality crowd movements, aggregating all heterogeneous spatial and temporal features. Finally, the planner outputs the next timestep action by a decoder.

B. Spatio-Temporal Graph Representation

We represent the socially aware navigation scenario as a ST-graph $\mathcal{G} = (\mathcal{N}, \mathcal{E}, \mathbf{M})$, \mathcal{N} is the node of agents. The robot policy and observed human states are factorized into robot nodes or human nodes. \mathcal{E}_S is the spatial edge represented by the spatial transformer parameter matrix \mathbf{M}_S , \mathcal{E}_T is the temporal edge represented by the temporal transformer parameter matrix \mathbf{M}_T . $\mathbf{M} \in \mathbb{R}^{N \times N}$ is the adjacency matrix constructed using a Gaussian kernel. The environmental representation \mathcal{F} is deconstructed based on a cross-hybrid spatio-temporal graph transformer. Once the environmental dynamics are built by a graph, the robot action vector \mathcal{A}_r can be calculated as follows:

$$\mathcal{A}_r = \mathcal{F}(\mathbf{s}_1^{\text{in}}, \dots, \mathbf{s}_t^{\text{in}}; \mathcal{G}). \quad (2)$$

C. NaviSTAR Architecture

Overview: As shown in Fig. 2, we develop a transformer-based framework to construct environmental dynamics representation using a ST-graph. First, the environment state $\mathbf{E} = [\mathbf{s}_1^{\text{in}}, \dots, \mathbf{s}_t^{\text{in}}]$ is fed as input into the network, which include all agents' observed states from the robot's field of view (FOV) during timestep 1 to timestep t. Then, a spatial-temporal graph transformer network is introduced to capture long-term spatial and temporal dependencies, with spatial attention maps and temporal attention maps. Finally, in order to fuse the cross-modality interactions, a multi-modal transformer is adapted to capture the multimodality of crowd navigation environment by aggregating all heterogeneous spatial attention maps and temporal attention maps from each agents (as shown in Fig. 4). The robot obtains the value V_{st} and the policy $\pi_{(a_t | s_t)}$ from a decoder.

Spatial Transformer Block: The spatial-temporal transformer block calculates the spatial attention and temporal attention separately from the environment state matrix, which is used to represent the edges of spatio-temporal graph. In the spatial transformer, we rotate the input matrix to align each agent's state with the same timestep to calculate the spatial dependencies. This encode the spatial attentions map (representing the importance of neighboring agents)

and spatial relational features (capturing the distance and relative orientation among pairwise agents) by the multi-head attention block and graph convolution layer. As shown in Fig. 3(a) the environment state $\mathbf{E} \in \mathbb{R}^{T \times N \times d}$ is fed into a fully connected layer to embed the positional information based on [19] to compute the spatial embeddings $\mathbf{E}_s = [\hat{\mathbf{s}}_1^{\text{in}}, \dots, \hat{\mathbf{s}}_t^{\text{in}}]$. Similarly, the temporal embeddings $\mathbf{E}_t = [\hat{\mathbf{s}}_1^{\text{tj}}, \dots, \hat{\mathbf{s}}_n^{\text{tj}}]$ are aligned by a fully connected layer in the temporal transformer block, as shown in Fig. 3(b). The spatial embeddings of each timestep $\hat{\mathbf{s}}^{\text{in}} \in \mathbb{R}^{N \times d}$ are then used as input for the spatial transformer.

In order to capture the spatial relational dependencies in each timestep, we introduce a graph convolution neural network (GCN) based on Chebyshev polynomial approximation [20]. This GCN is used to generate the static spatial relations $\hat{\mathbf{h}}^G \in \mathbb{R}^{N \times d}$ among multiple agents,

$$\hat{\mathbf{h}}^G = \sum_{k=0}^K \theta_k \mathbf{T}_k(\hat{\mathbf{L}}) \hat{\mathbf{s}}^{\text{in}} \quad (3)$$

where \mathbf{I}_n, \mathbf{D} is an identity matrix and the diagonal degree matrix of the adjacency matrix \mathbf{M} . The symmetric normalized Laplacian matrix is then calculated as $\mathbf{L} = \mathbf{I}_n - \mathbf{D}^{-\frac{1}{2}} \mathbf{M} \mathbf{D}^{\frac{1}{2}}$. After that, the scaled Laplacian matrix is defined as $\hat{\mathbf{L}} = 2\mathbf{L}/\lambda_{\max} - \mathbf{I}_n$, where λ_{\max} is the largest eigenvalue of \mathbf{L} . The parameter θ is a weighted parameter, and K is the kernel size of the graph convolution. Finally, the result $\hat{\mathbf{h}}^G$ is calculated by Chebyshev polynomials \mathbf{T}_k .

Even though GCN can capture static spatial relational features, the robot needs to understand potential dynamic spatial features with respect to adjacent agents' intents and attentions. Thus, we utilize multi-head attention mechanism to generate each agents' spatial attention maps, as shown in Fig. 4, to capture the dynamic spatial dependencies $\hat{\mathbf{h}}^{\text{SM}}$.

$$\text{Atten} \left(\mathbf{Q}_{\text{ST}}^{(i)}, \mathbf{K}_{\text{ST}}^{(i)} \mathbf{V}_{\text{ST}}^{(i)} \right) = \frac{\text{softmax} \left(\mathbf{Q}_{\text{ST}}^{(i)} \mathbf{K}_{\text{ST}}^{(i)\top} \right)}{\sqrt{d_h}} \cdot \mathbf{V}_{\text{ST}}^{(i)} \quad (4)$$

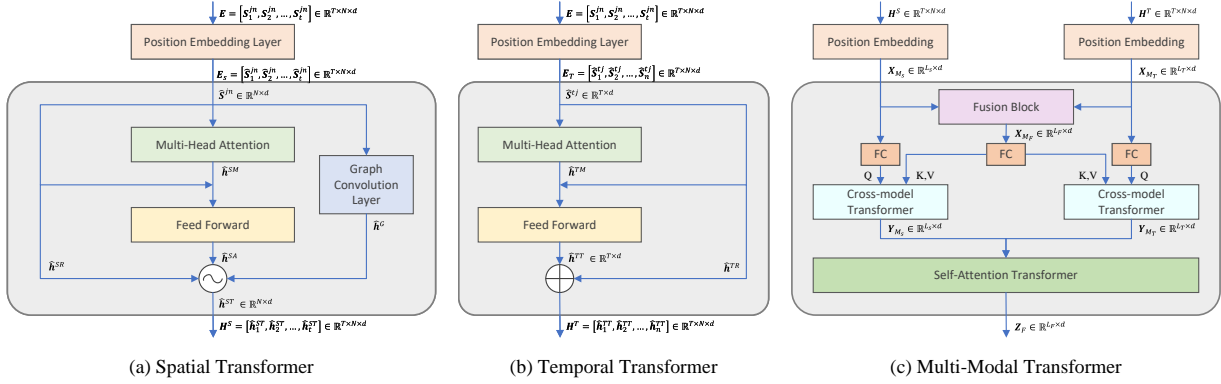


Fig. 3: NaviSTAR neural network framework: (a) Spatial Transformer leverages a multi-head attention layer and a graph convolution network along the time-dimension to represent spatial attention features and spatial relational features; (b) Temporal Transformer utilizes multi-head attention layers to capture each individual agent's long-term temporal attention dependencies; and (c) Multi-Modal Transformer fuses heterogeneous spatial and temporal features via a multi-head cross-modal transformer block and a self-transformer block to abstract the uncertainty of multimodality crowd movements.

$$\text{Multi} \left(\mathbf{Q}_{\text{ST}}^{(i)}, \mathbf{K}_{\text{ST}}^{(i)}, \mathbf{V}_{\text{ST}}^{(i)} \right) = f_{\text{fc}}(\text{head}_1, \dots, \text{head}_h) = \hat{\mathbf{h}}^{\text{SM}},$$

$$\text{head}_{(\cdot)} = \text{Atten}_{(\cdot)} \left(\mathbf{Q}_{\text{ST}}^{(i)}, \mathbf{K}_{\text{ST}}^{(i)}, \mathbf{V}_{\text{ST}}^{(i)} \right) \quad (5)$$

where $f_{\text{fc}}()$ is a linear function, and h is the number of heads in the multi-head attention mechanism, i is the label of timesteps in the spatial transformer, while it represents the label of pedestrians in the temporal transformer. $\mathbf{Q}_{\text{ST}}^{(i)}, \mathbf{K}_{\text{ST}}^{(i)}, \mathbf{V}_{\text{ST}}^{(i)}$ are query, key and value matrices with dimension d_h , which are computed from \hat{s}^{in} or \hat{s}^{tj} in the spatial transformer or temporal transformer block. They are generated using a fully connected layer with respect to parameter matrices $\{\mathbf{M}_S, \mathbf{M}_T\}$.

We use the rectified linear unit (ReLU) activation function to capture non-linear features in the feedforward network. Additionally, residual connections are added to the spatial and temporal transformer networks to accelerate convergence and stabilize the framework [21].

$$\hat{\mathbf{h}}^{\text{SR}} = \hat{\mathbf{h}}^{\text{SM}} + \hat{s}^{\text{in}} \quad (6)$$

$$\hat{\mathbf{h}}^{\text{SA}} = \hat{\mathbf{h}}^{\text{SR}} + \text{ReLU}(\text{ReLU}(\hat{\mathbf{h}}^{\text{SR}} \mathbf{W}_S^{(1)}) \mathbf{W}_S^{(2)}) \mathbf{W}_S^{(3)} \quad (7)$$

where $\mathbf{W}_S^{(1)}, \mathbf{W}_S^{(2)}, \mathbf{W}_S^{(3)}$ are the weight matrices of the hidden layers in the feedforward network.

Lastly, a gate mechanism d is used to combine the representation of spatial features $\hat{\mathbf{h}}^{\text{ST}}$,

$$d = \text{sigmoid} \left[f_{\text{fc}}(\hat{\mathbf{h}}^{\text{SA}}) + f_{\text{fc}}(\hat{\mathbf{h}}^G) \right] \quad (8)$$

$$\mathbf{h}^{\text{ST}} = d \cdot (\hat{\mathbf{h}}^{\text{SA}}) + (1 - d) \cdot (\hat{\mathbf{h}}^G) \quad (9)$$

Then, we pack up the final spatial features $\hat{\mathbf{h}}^{\text{ST}}$ in a spatial attention matrix $\mathbf{H}^S = [\hat{\mathbf{h}}_1^{\text{ST}}, \dots, \hat{\mathbf{h}}_t^{\text{ST}}] \in \mathbb{R}^{T \times N \times d}$.

Temporal Transformer Block: Due to the highly motion-dependency of the temporal dimension, we designed temporal edges connecting each agent's context pair-wise across timesteps. For example, since motion is continuous, we can predict future velocity and position based on current trajectory history. In the temporal transformer block, we set each agent's individual trajectory as a row vector of input. As shown in Fig. 3(b), the temporal transformer block is similar to the spatial transformer, but without a GCN. Firstly, the

temporal embeddings \mathbf{E}_t are fed into a multi head attention layer to capture temporal features $\hat{\mathbf{h}}^{\text{TM}}$ and create temporal attention maps for each agents as shown in Fig. 4 from each agent's trajectory data. Next, a feedforward network and residual connection structure are deployed in the framework to obtain the final temporal dependencies $\hat{\mathbf{h}}^{\text{TT}}$, which is same as the spatial transformer.

$$\hat{\mathbf{h}}^{\text{TR}} = \hat{\mathbf{h}}^{\text{TM}} + \hat{s}^{\text{tj}} \quad (10)$$

$$\hat{\mathbf{h}}^{\text{TT}} = \hat{\mathbf{h}}^{\text{TR}} + \text{ReLU}(\text{ReLU}(\hat{\mathbf{h}}^{\text{TR}} \mathbf{W}_T^{(1)}) \mathbf{W}_T^{(2)}) \mathbf{W}_T^{(3)} \quad (11)$$

where $\mathbf{W}_T^{(1)}, \mathbf{W}_T^{(2)}, \mathbf{W}_T^{(3)}$ are the weight matrices of the hidden layers in the feedforward network. Finally, we package the temporal feature $\hat{\mathbf{h}}^{\text{TT}}$ into a temporal attention matrix $\mathbf{H}^T = [\hat{\mathbf{h}}_1^{\text{TT}}, \dots, \hat{\mathbf{h}}_n^{\text{TT}}] \in \mathbb{R}^{T \times N \times d}$.

Multi-Modal Transformer Block: In order to capture the multimodalities and uncertainty of crowd movements, we have developed a multi-head multi-modal transformer block that fuses the heterogeneous spatial and temporal attention maps of each agents and captures long-range dependencies among modalities. Inspired by [16], [18], we utilize a multi-head cross-modal transformer to calculate the high-level representation of environmental dynamics. As shown in Fig. 3(c), first, the spatial and temporal feature matrices ($\mathbf{H}^S, \mathbf{H}^T$) are separately processed by a positional embedding layer from [19] to ensure order-invariance, resulting in $\mathbf{X}_{M_S} \in \mathbb{R}^{L_S \times d}$, $\mathbf{X}_{M_T} \in \mathbb{R}^{L_T \times d}$. Next, the spatial and temporal feature matrices are concatenated by a fusion block as $\mathbf{X}_{M_F} \in \mathbb{R}^{L_F \times d}$ to formulate the unimodal Query \mathbf{Q}_U , fusion Key \mathbf{K}_F and fusion Value \mathbf{V}_F by a fully connected layer as follows:

$$\mathbf{Q}_U = \mathbf{X}_{M_g} \cdot \mathbf{W}_{Q_U}$$

$$\mathbf{K}_F = \mathbf{X}_{M_F} \cdot \mathbf{W}_{K_F}$$

$$\mathbf{V}_F = \mathbf{X}_{M_F} \cdot \mathbf{W}_{V_F} \quad (12)$$

where $\mathbf{W}_{Q_U} \in \mathbb{R}^{d \times d_k}$, $\mathbf{W}_{K_F} \in \mathbb{R}^{d \times d_k}$ and $\mathbf{W}_{V_F} \in \mathbb{R}^{d \times d_v}$ are learnable weights of the multi modal transformer.

Secondly, the unimodal feature \mathbf{X}_{M_g} is fed into multi-head cross-modal attention block with the fusion feature \mathbf{X}_{M_F} to capture high-level HRI embedding, aggregating each agent's spatial and temporal attention maps, with $g \in \{S, T\}$. And

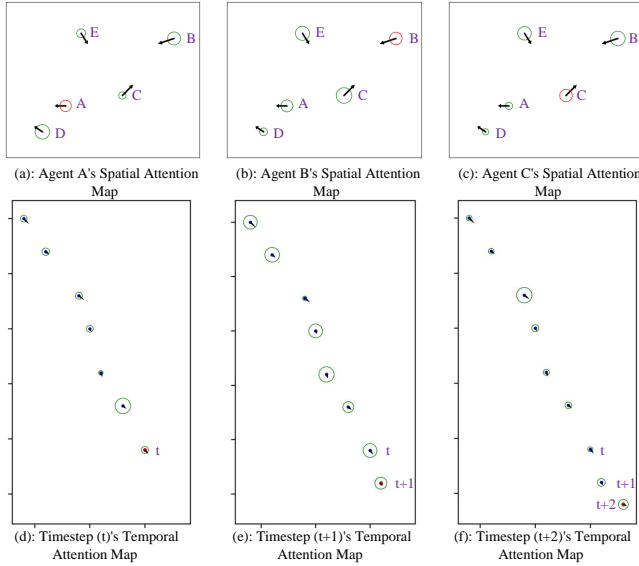


Fig. 4: An illustration of spatial attention maps and temporal attention maps: sub-figures (a), (b), and (c) exhibit the spatial attention maps from different agents at the same timestep; (d), (e), and (f) present the temporal attention maps from different timesteps in the same agent's view. The radius of the circle represents the importance level based on the perceptive of the agent represented by the red circle.

the $\mathbf{Y}_{M_g}^{Mul}$ is the output of multi-head cross-modal attention layer in the cross-modal transformer as follows:

$$\begin{aligned} \mathbf{Y}_{M_g}^{\text{head}_j} &= \text{CMAtten}(\mathbf{X}_{M_g}) \\ &= \text{Atten}(\mathbf{Q}_U^{\text{head}_j}, \mathbf{K}_F^{\text{head}_j}, \mathbf{V}_F^{\text{head}_j}) \\ &= \text{softmax}\left(\frac{\mathbf{Q}_U^{\text{head}_j}(\mathbf{K}_F^{\text{head}_j})^\top}{\sqrt{d_k}}\right) \cdot \mathbf{V}_F^{\text{head}_j} \end{aligned} \quad (13)$$

$$\mathbf{Y}_{M_g}^{Mul} = f_{fc}(\mathbf{Y}_{M_g}^{\text{head}_1}, \dots, \mathbf{Y}_{M_g}^{\text{head}_h}) \quad (14)$$

Additionally, we incorporate a residual connection mechanism and feedforward layers into the cross-modal transformer block, based on [18]. The output of the multi modal transformer \mathbf{Y}_{M_g} is defined as:

$$\mathbf{Y}_{M_g} = \text{Trans}_{\text{cross}}(\mathbf{X}_{M_g}, \mathbf{Y}_{M_g}^{Mul}). \quad (15)$$

Finally, the crossed spatial feature and crossed temporal feature are adapted by an original transformer network [19] to further improve the efficiency of cross-modal fusion and adjust for noise. A fully-connected layer-based decoder is then designed to extract the value V_{s_t} and the policy $\pi_{(a_t|s_t)}$ from the self-attention layer output $\mathbf{Z}_F \in \mathbb{R}^{L_F \times d}$.

$$\mathbf{Z}_F = \text{Trans}_{\text{self}}(\mathbf{Y}_{M_S}, \mathbf{Y}_{M_T}). \quad (16)$$

Preference Learning and Reinforcement Learning:

In the training processing, we use preference learning [22] and an off-policy RL algorithm, soft actor critic (SAC) [23], to implicitly encode social norms and human expectations into the reward function, policy, and value function, based on [11].

Preference learning is a kind of active learning, which aligns a reward neural network with human preferences that a human supervisor selects from different trajectory segments. Let ε be a segment of a trajectory $[s_n, a_n, \dots, s_{n+t}, a_{n+t}]$,

and ω be a preference based on a distribution $[(0,1), (1,0), (0.5,0.5)]$. Firstly, two segments are displayed to the human supervisor which are sampled from the replay buffer. Then, the supervisor can select one to update the replay buffer \mathcal{B} with human preferences, by a tuple $\langle \varepsilon_0, \varepsilon_1, \omega \rangle$, where $(1,0)$ and $(0,1)$ indicate left or right is better, and $(0.5,0.5)$ represents other situations (such as nonjudgmental). The preference predictor \mathcal{P} is defined as follows:

$$\mathcal{P}(\alpha) [\varepsilon_1 > \varepsilon_0] = \frac{\exp \sum_t \tilde{r}_\alpha (\mathbf{s}_t^1, \mathbf{a}_t^1)}{\sum_{u \in \{0,1\}} \exp \sum_t \tilde{r}_\alpha (\mathbf{s}_t^u, \mathbf{a}_t^u)} \quad (17)$$

$$\omega = \begin{cases} (1, 0), & \mathcal{P}(\alpha) [\varepsilon_0 > \varepsilon_1] > \frac{1}{2} \\ (0, 1), & \mathcal{P}(\alpha) [\varepsilon_1 > \varepsilon_0] > \frac{1}{2} \\ (0.5, 0.5), & |\mathcal{P}(\alpha) [\varepsilon_0 > \varepsilon_1] - \mathcal{P}(\alpha) [\varepsilon_1 > \varepsilon_0]| \leq 0.1 \end{cases} \quad (18)$$

where \tilde{r} is the learnable reward function from preferences.

And then, a loss function $\mathcal{L}_{(\alpha)}^R$ is deployed to update the reward function network from the predictor with respect to real human feedback as follows:

$$\mathcal{L}_{(\alpha)}^R = - \mathbb{E}_{(\varepsilon_0, \varepsilon_1, \omega) \sim \mathcal{B}} \omega(0) \log \mathcal{P}(\alpha) [\varepsilon_0 > \varepsilon_1] + \omega(1)$$

$$\mathcal{P}(\alpha) [\varepsilon_1 > \varepsilon_0] + \omega(0.5) (\mathcal{P}(\alpha) [\varepsilon_1 > \varepsilon_0] + \mathcal{P}(\alpha) [\varepsilon_0 > \varepsilon_1]). \quad (19)$$

Once the reward function \tilde{r} is trained, the off-policy RL algorithm SAC is used to update value function V and the policy π , we use function.[17],[18],[19] to develop [11], as our training procedure.

IV. EXPERIMENTS AND RESULTS

A. Simulation Experiment

1) *Simulation Environment*: Fig. 6 illustrates our 2D simulation environment, which is based on [7], [9]. The environment dynamics are kinematically simplified using Δt as described in [6], and human policies are based on ORCA [24]. We assume that the robot is invisible to each human in the environment to optimize navigation behavior. The robot's actions are defined as $\mathbf{a}_t = [v_x, v_y]$, and its FOV is set from 0° to 360° . We train and test the simulation in an open space with dimensions of $20 m \times 22 m$, where humans are randomly generated on a circle with a radius of $8 m$.

2) *Baseline and Ablation Models*: To ensure fair comparison, we selected several baseline methods: ORCA as the traditional method, CADRL [6] and SARL [7] as the deep V-learning baseline, RGL [8] as the model-based RL baseline, and SRNN [9] as the ST-graph algorithm baseline. To eliminate the effect of RL parameters, we implemented two ablation models. The first ablation model, called Nav-iSRNN, uses the preference learning and SAC training procedure based on the SRNN interaction network to evaluate the differences in the interaction network under the same conditions. The second ablation model, called STAR+PPO, employs a handcrafted reward function as described in [6] and the training procedure from [9]. We did not use FAPL [11] as a baseline because its interaction network is similar to our ablation model.

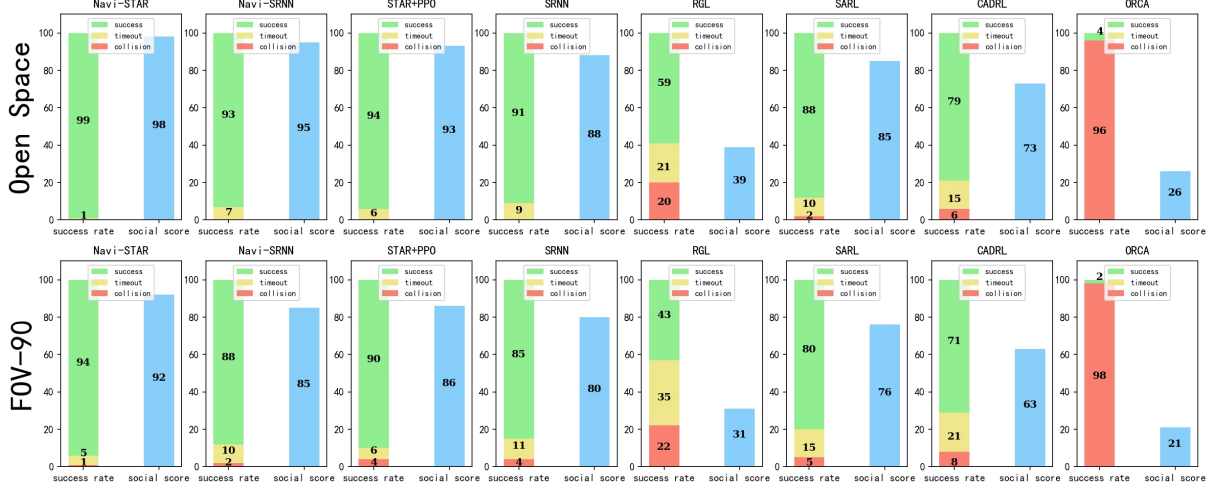


Fig. 5: Simulation tests: the success rate (green) and social score (blue) of each policy from 500 tests with the same environment configuration (Open Space or FOV-90°).

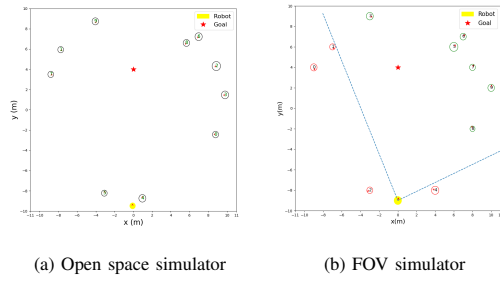


Fig. 6: An illustration of the simulator: (a) We designed a gym-based simulator in the experiment section, which is a $22\text{ m} \times 20\text{ m}$ open space. In the simulator, the robot is represented by a yellow circle, and humans are abstracted by white circles with different social radii. The goal position of the robot is denoted by a red star; (b) The robot's FOV is shown in a similar environment, which displays observable agents as green circles and unobserved agents as red circles.

3) *Training Details*: All the baseline algorithms are trained following their original papers and initial configurations. And then we tested all the policies in the same environment and parameters. We also set the same configuration for each ablation models, with 4×10^{-5} of learning rate trained in 1×10^4 episodes.

4) *Evaluation Approaches*: As shown in Fig. 5, we utilize two kinds of evaluation methods. The first one is a successful rate, which collects the number of successful cases from total of 500 test cases. And we designed an evaluation function (social score F_{SC}) to estimate the comprehensive performance of social navigation, which considers the navigation time, the dangerous segments percentage, and the uncomfortable level of the robotic path.

$$F_{SC} = 100 \cdot [v \cdot F_{time} + (1 - v) \cdot F_{uc} + v' \cdot FF] \quad (20)$$

where $v \in [0, 1]$ is an evaluation parameter, which affects the rate of navigation time and social assessment in the social score, and $v' \in (\infty, 0]$ is a penalty factor, which represents the importance of failure rate with FF in the social score function. And the FF is the collision and overtime rate.

Final, the social score is normalized in $F_{SC} \in (-\infty, 100]$ 100 points. In our experiments, the v is 0.35 and v' is 0.25.

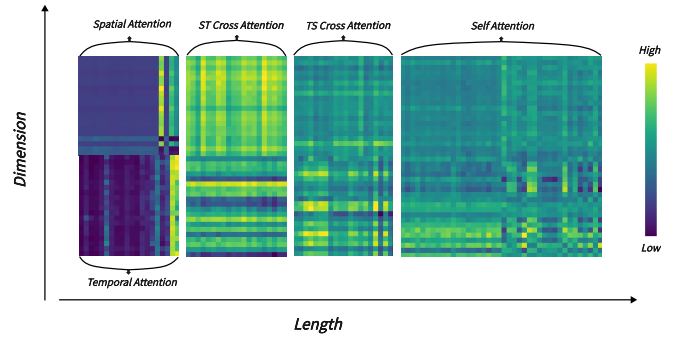


Fig. 7: Attention visualization: Visualization of a NaviSTAR attention weight group example consisting of spatial and temporal attention matrices at the result of the spatial and temporal transformer, cross attention matrices at the final layer of the multi-modal transformer, and a final attention matrix from the self-attention transformer.

The F_{time} is defined as:

$$F_{time} = 1 - \frac{1}{n} \sum_{l=1}^n \frac{1 - \min}{\max - \min} \quad (21)$$

where n is the number of successful cases in the test, l is the navigation time of l -th successful paths, \min is the minimum cost of time in total cases, and \max is the maximum time of successful path. We normalize the $F_{time} \in [0, 1]$.

$$F_{uc} = 1 - \frac{1}{2} \cdot \left[\frac{1}{m} \cdot \sum_{o=1}^m \text{sigmoid} \left(\frac{du \cdot \Delta t}{\int^T dis \cdot dt} - 1 \right) + \frac{n}{m} \right] \quad (22)$$

where m is the number of instances who are involved with uncomfortable segments, and du is the uncomfortable distance which is set as 0.45m in our environment from [25], and dis is the min-distance between robot and each pedestrian. The integral is a weighted average of robot dis from all the cases. Finally, we normalize the $F_{uc} \in [0, 1]$ by a standard nonlinear function to evaluate the average impact caused by dangerous segments.

B. Qualitative Analysis

1) *Overall*: NaviSTAR demonstrated better performance due to its powerful interaction neural network, which can im-

plicitly encode deeper potential interactions and cooperation among humans and robot. As shown in Fig. 4, NaviSTAR aggregates all the spatial and temporal attention maps from each individual agent. Fig. 7 shows the visualization of attention matrices where each cell represents an attention score between two feature blocks. The spatial attention matrix shows the relative importance of each agent to its surroundings in each timestep, while the temporal matrix presents the importance of all agents’ self-trajectory states. The cross-attention matrix and self-attention matrix abstract the results of the fusion to capture environmental dynamics.

We compared the success rate and social score of all algorithms under the same configuration, which includes 10 humans and 18 m of target distance, in an open space with FOV-90° conditions separately, using 500 random tests, as shown in Fig. 5 Table I presents the social scores with a different single parameter.

TABLE I: Social Score Table

Methods	Social Score			Social Score		
	90	180	360	Human Number	10	15
ORCA [24]	21.1	23.2	27.4	29.2	25.7	22.6
CADRL [6]	62.7	65.4	69.6	77.1	73.2	70.1
SARL [7]	31.3	34.1	39.7	42.2	39.1	36.7
RGL [8]	76.5	81.3	84.9	90.3	88.3	86.6
SRNN [9]	80.4	84.7	88.6	87.1	84.8	81.2
STAR+PPO	85.1	88.9	91.3	99.2	95.4	94.3
NaviSRNN	89.3	91.6	94.5	95.7	93.4	91.2
NaviSTAR	91.7	93.1	94.2	98.9	98.5	95.8

2) *Traditional Methods*: As shown in Fig. 5 and Table I, the traditional methods cannot be well deployed in a crowded environment with the assumption of the invisible robot. In our tests, ORCA shows the lowest success rate by a one-step avoidance policy in a dynamic environment because of the short-sight. Except for the failure cases, ORCA also represented a bad social performance, since the robot could not understand the deeper interactions.

3) *Learning-based Methods*: In Fig. 5 and Table I, CADRL and SARL, as previous learning-based socially aware navigation approaches, showed limited performance and social compliance because they cannot capture deeper and full HRI. Secondly, we adapted the original configuration for the RGL planner. However, RGL did not demonstrate good performance, possibly due to the complex parameter engineering of model-based RL. Thirdly, compared to other baseline algorithms, SRNN demonstrated better interaction reasoning ability using an ST-graph and recurrence framework that can describe the spatial and temporal relationship of the crowd. However, due to the limitations of the handcrafted reward function, SRNN does not consider more social norms. Additionally, a few SRNN success cases timed out because SRNN sometimes cannot capture long-term dependencies.

4) *Ablation Models*: Based on the trajectories shown in Fig. 8, we can observe that NaviSTAR has learned to navigate through the side with fewer potential risks by taking into account the crowd intent, while NaviSRNN continues to follow its previous plan with higher collision risks, even at early timesteps. This suggests that the spatio-temporal

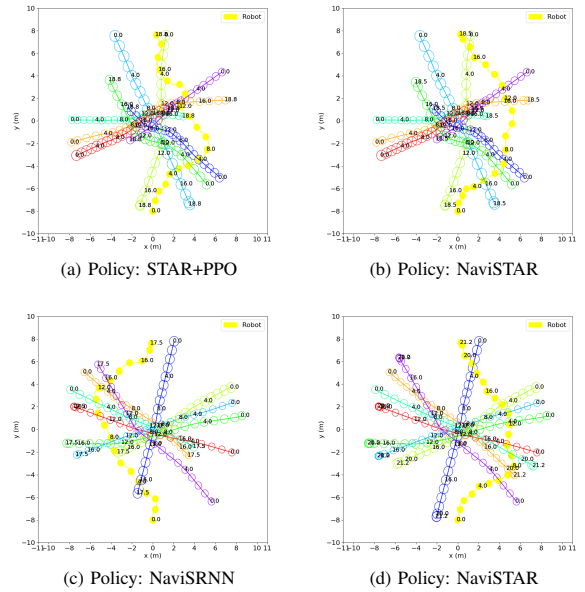


Fig. 8: Simulation tests: The trajectories of the first row are tested by a same case in open space, and the second row is tested by another case in FOV-90°.

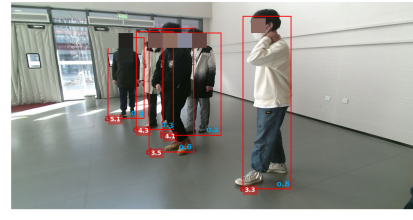


Fig. 9: A robotic perception illustration: The velocity and distance predictors (left) present the distance between the robot and pedestrians as a red number and estimate the velocity of pedestrians as a blue number. The robotic 2D local map (right) shows the relative localization of pedestrians with velocity direction. An objective detector is deployed to capture the labels of users.

graph transformer used in NaviSTAR has better abilities to reason about long-term dependencies compared to SRNN’s network. Furthermore, NaviSTAR and STAR+PPO are good at interaction representation to navigate along a safer way, but NaviSTAR demonstrates better social norm compliance than STAR+PPO, which NaviSTAR dodges almost pedestrians. These findings suggest that incorporating a spatio-temporal graph transformer network and active reward learning framework can significantly improve the performance and social compliance of socially aware navigation algorithms in human-filled environments.

C. Real-world Experiment

We also conducted real-world tests with 8 participants (1 female and 7 males, all aged over 18)². The robot and participants followed the same behavior policy, starting point, and end goal in each test, and the planner of the robot was unknown and randomized for participants. Pre-experiment and post-experiment usability questionnaires were distributed to collect background data and feedback on the robot. We

²This user study was reviewed by the BUCT Institutional Review Board (IRB)

developed a robotic perception system that utilized a velocity predictor based on YOLO with Deepsort [26] and a distance estimator from [27], as shown in Figure 9. We selected NaviSTAR, NaviSRNN, STAR+PPO and SRNN as baselines for the user study. In the training procedures of NaviSTAR and ablation models, over 10 human supervisors selected 5000 preferences of segments. During the testing phase, we deployed a mobile robot with Kinect V2 in an 86° FOV. All algorithms were tested with the same configuration, and each algorithm was tested by 5 times.

The evaluation of real world tests consisted of comfort and naturalness from users' feedback, with responses ranging from strongly disagree (1) to strongly agree (5). We collected the results based on participants' experiences interacting with the robot. Two factors were summed together, and then multiplied by 10 to be mapped to the range [20, 100]. According to the feedback received, NaviSTAR had an average score of 93, which was higher than NaviSRNN's score of 89, STAR+PPO's score of 86, and SRNN's score of 80. More details about this user study setting and results can be found on our website¹.

V. CONCLUSION

In this paper, we presented NaviSTAR, a novel benchmark for socially aware navigation that incorporates a cross-hybrid spatial-temporal transformer network to understand crowd interactions and active reward learning to learn social norms and guidance from a supervisor. Our policy was trained using the procedure from [11], and we have also developed a new evaluation function for socially aware navigation. Through extensive experiments in both simulator and real-world scenarios, we demonstrated that NaviSTAR outperforms previous methods with outstanding performance. We believe that our algorithm has the potential to make people feel more comfortable with robots navigating in shared environments.

REFERENCES

- [1] A. Garrell and A. Sanfeliu, "Cooperative social robots to accompany groups of people," *The International Journal of Robotics Research*, vol. 31, no. 13, pp. 1675–1701, 2012.
- [2] N. E. Du Toit and J. W. Burdick, "Robot motion planning in dynamic, uncertain environments," *IEEE Transactions on Robotics*, vol. 28, no. 1, pp. 101–115, 2011.
- [3] M. Bennewitz, W. Burgard, G. Cielniak, and S. Thrun, "Learning motion patterns of people for compliant robot motion," *The International Journal of Robotics Research*, vol. 24, no. 1, pp. 31–48, 2005.
- [4] P. Trautman, J. Ma, R. M. Murray, and A. Krause, "Robot navigation in dense human crowds: Statistical models and experimental studies of human–robot cooperation," *The International Journal of Robotics Research*, vol. 34, no. 3, pp. 335–356, 2015.
- [5] H. Kretzschmar, M. Spies, C. Sprunk, and W. Burgard, "Socially compliant mobile robot navigation via inverse reinforcement learning," *The International Journal of Robotics Research*, vol. 35, no. 11, pp. 1289–1307, 2016.
- [6] Y. F. Chen, M. Liu, M. Everett, and J. P. How, "Decentralized non-communicating multiagent collision avoidance with deep reinforcement learning," in *2017 IEEE international conference on robotics and automation (ICRA)*. IEEE, 2017, pp. 285–292.
- [7] C. Chen, Y. Liu, S. Kreiss, and A. Alahi, "Crowd-robot interaction: Crowd-aware robot navigation with attention-based deep reinforcement learning," in *2019 international conference on robotics and automation (ICRA)*. IEEE, 2019, pp. 6015–6022.
- [8] C. Chen, S. Hu, P. Nikdel, G. Mori, and M. Savva, "Relational graph learning for crowd navigation," in *2020 IEEE/RSJ International Conference on Intelligent Robots and Systems (IROS)*. IEEE, 2020.
- [9] S. Liu, P. Chang, W. Liang, N. Chakraborty, and K. Driggs-Campbell, "Decentralized structural-rnn for robot crowd navigation with deep reinforcement learning," in *2021 IEEE International Conference on Robotics and Automation (ICRA)*. IEEE, 2021, pp. 3517–3524.
- [10] M. Sun, F. Baldini, P. Trautman, and T. Murphey, "Move Beyond Trajectories: Distribution Space Coupling for Crowd Navigation," in *Proceedings of Robotics: Science and Systems*, Virtual, July 2021.
- [11] R. Wang, W. Wang, and B.-C. Min, "Feedback-efficient active preference learning for socially aware robot navigation," in *2022 IEEE/RSJ International Conference on Intelligent Robots and Systems (IROS)*. IEEE, 2022, pp. 11336–11343.
- [12] S. Liu, P. Chang, Z. Huang, N. Chakraborty, W. Liang, J. Geng, and K. Driggs-Campbell, "Socially aware robot crowd navigation with interaction graphs and human trajectory prediction," *arXiv preprint arXiv:2203.01821*, 2022.
- [13] C. Yu, X. Ma, J. Ren, H. Zhao, and S. Yi, "Spatio-temporal graph transformer networks for pedestrian trajectory prediction," in *European Conference on Computer Vision*. Springer, 2020, pp. 507–523.
- [14] Z. Li, W. Wang, H. Li, E. Xie, C. Sima, T. Lu, Y. Qiao, and J. Dai, "Bevformer: Learning bird's-eye-view representation from multi-camera images via spatiotemporal transformers," in *Computer Vision–ECCV 2022: 17th European Conference, Tel Aviv, Israel, October 23–27, 2022*. Springer, 2022, pp. 1–18.
- [15] C. Chen, Y. Liu, L. Chen, and C. Zhang, "Bidirectional spatial-temporal adaptive transformer for urban traffic flow forecasting," *IEEE Transactions on Neural Networks and Learning Systems*, 2022.
- [16] Y.-H. H. Tsai, S. Bai, P. P. Liang, J. Z. Kolter, L.-P. Morency, and R. Salakhutdinov, "Multimodal transformer for unaligned multimodal language sequences," in *Proceedings of the conference. Association for Computational Linguistics. Meeting*, vol. 2019. NIH Public Access, 2019, p. 6558.
- [17] R. J. Chen, M. Y. Lu, W.-H. Weng, T. Y. Chen, D. F. Williamson, T. Manz, M. Shady, and F. Mahmood, "Multimodal co-attention transformer for survival prediction in gigapixel whole slide images," in *Proceedings of the IEEE/CVF International Conference on Computer Vision*, 2021, pp. 4015–4025.
- [18] R. Wang, W. Jo, D. Zhao, W. Wang, B. Yang, G. Chen, and B.-C. Min, "Husformer: A multi-modal transformer for multi-modal human state recognition," *arXiv preprint arXiv:2209.15182*, 2022.
- [19] A. Vaswani, N. Shazeer, N. Parmar, J. Uszkoreit, L. Jones, A. N. Gomez, Ł. Kaiser, and I. Polosukhin, "Attention is all you need," *Advances in neural information processing systems*, vol. 30, 2017.
- [20] T. N. Kipf and M. Welling, "Semi-supervised classification with graph convolutional networks," in *International Conference on Learning Representations*, 2017. [Online]. Available: <https://openreview.net/forum?id=SUJ4ayYg1>
- [21] K. He, X. Zhang, S. Ren, and J. Sun, "Deep residual learning for image recognition," in *Proceedings of the IEEE conference on computer vision and pattern recognition*, 2016, pp. 770–778.
- [22] K. Lee, L. Smith, A. Dragan, and P. Abbeel, "B-pref: Benchmarking preference-based reinforcement learning," in *Thirty-fifth Conference on Neural Information Processing Systems Datasets and Benchmarks Track (Round 1)*, 2021. [Online]. Available: <https://openreview.net/forum?id=ps95-mkHF>
- [23] T. Haarnoja, A. Zhou, P. Abbeel, and S. Levine, "Soft actor-critic: Off-policy maximum entropy deep reinforcement learning with a stochastic actor," in *International conference on machine learning*. PMLR, 2018, pp. 1861–1870.
- [24] J. Van Den Berg, S. J. Guy, M. Lin, and D. Manocha, "Reciprocal n-body collision avoidance," in *Robotics Research: The 14th International Symposium ISRR*. Springer, 2011, pp. 3–19.
- [25] J. Rios-Martinez, A. Spalanzani, and C. Laugier, "From proxemics theory to socially-aware navigation: A survey," *International Journal of Social Robotics*, vol. 7, pp. 137–153, 2015.
- [26] A. Pramanik, S. K. Pal, J. Maiti, and P. Mitra, "Granulated rcnn and multi-class deep sort for multi-object detection and tracking," *IEEE Transactions on Emerging Topics in Computational Intelligence*, vol. 6, no. 1, pp. 171–181, 2021.
- [27] L. Bertoni, S. Kreiss, T. Mordan, and A. Alahi, "Monstereo: When monocular and stereo meet at the tail of 3d human localization," in *2021 IEEE International Conference on Robotics and Automation (ICRA)*. IEEE, 2021, pp. 5126–5132.